11-1-2021

Effect of Non-Uniform Temperature Exposure on the Out-of-Plane Bending Performance of Ordinary Laminated Glass Panels

Maged A. Youssef
Western University, youssef@uwo.ca

Ajitanshu Vedrtnam
Invertis University

Chiara Bedon
University of Trieste

Shashikant Chaturvedia
Invertis University

Citation of this paper:
Vedrtnam A, Bedon C, **Youssef MA**, Chaturvedia S, 2021, "Effect of Non-Uniform Temperature Exposure on the Out-of-Plane Bending Performance of Ordinary Laminated Glass Panels", Composite Structures, 275: 114517, https://doi.org/10.1016/j.compstruct.2021.114517.

Effect of Non-Uniform Temperature Exposure on the Out-of-Plane Bending Performance of Ordinary Laminated Glass Panels

Ajitanshu Vedrtnam [1*], Chiara Bedon [2], Maged A Youssef [3], Shashikant Chaturvedi [1]

[1] Invertis University, Department of Mechanical Engineering, Bareilly, UP, India-243001

[2] University of Trieste, Department of Engineering and Architecture, Trieste, Italy

[3] Western University, Department of Civil and Environmental Engineering, London, ON N6A 5B9, Canada

* ajitanshu.m@invertis.org

Effect of Non-Uniform Temperature Exposure on the Out-of-Plane Bending Performance of Ordinary Laminated Glass Panels

Abstract

Among the open design issues for structural laminated glass (LG) elements, their mechanical performance during fire exposure stands as a safety concern. This issue is the focus of this paper. An experimental investigation is conducted to evaluate the effect of non-uniform thermal gradients on the out-of-plane bending capacity of standard LG specimens. The pre-fracture, cracking, and post-fracture performances of LG panels were examined using a three-point bending setup. The bending tests were carried out on un-heated LG samples and heated samples, which were either hot or cooled down. The reliability of available analytical and numerical methods to predict the out-of-plane bending performance of LG is then investigated. The accuracy of the analytical and numerical methods was found to be highly affected by the non-uniform thermal boundaries, as well as by the assigned material properties, which are highly sensitive to the fire exposure.

Keywords: Laminated glass (LG); out-of-plane bending; thermal exposure; thermal history; numerical modelling

1. Introduction

The enhanced post-cracking performance of laminated glass (LG) has increased its use in architectural, automotive and defense applications in the last few decades [1]. Several research studies have focused on the in-plane and out-of-plane bending response of LG members under variable boundary and loading configurations. Those studies covered many issues including: (1) the definition of an effective thickness for multi-layered LG [2-4], (2) the development of novel treatment methods to improve the fatigue behaviour of LG [5-7], (3) the effects of interlayer type and stiffness on the flexural performance of LG [8-13], (4) the effects of the interlayer materials and their bond characteristics [14, 15], (5) the delamination strength of LG and its effect on the structural performance [16, 17], (6) the performance of LG exposed to impact [18-20] and blast loads [21-23], and (7) the post-cracked structural behaviour [24-26].

The thermal breakage of glass during fire exposure has been experimentally investigated at the component and assembly levels [27-37]. Thermal fracture of glass is known to depend on various parameters, like frame properties, fire location, glass type, coating, etc. For clear glazing, it was established that the thermal load, panel size, smoke movement, and installation approach strongly affect the collapse mechanism and load-bearing capacity during fire. The effect of non-uniform fire exposure on clear and tinted monolithic glass panels was investigated by Vedrtnam et al. [38]. The analysis of local effects in the glass and interlayer components is the first step to conduct numerical thermal analyses [39, 40] and to calibrate simplified design procedures to examine glass thermal shock [41].

The literature has mainly examined the thermal behaviour of vertical glass elements, which are used as curtain elements in buildings. The examined mechanical loads were, thus, minimum. Previous studies have mainly focused on thermal loading and did not address the major design challenges for glass elements exposed to mechanical loads. Bedon [42] summarized the current challenges, issues, and developments for glass systems exposed to fire, and provided a state of art on the material properties. The thermal conductivity and specific heat capacity of glass are known to increase with temperature, whereas the tensile strength and elastic modulus typically decrease [43]. This behaviour results in a progressive stiffness degradation, which complicates predicting the fire endurance for load-bearing glass elements [44]. The structural performance assessment of monolithic and LG requires detailed analysis of input parameters, including the thermo-physical and mechanical properties of materials, as well as thermal and mechanical boundaries.

The effect of elevated non-uniform temperature exposure on the load-bearing capacity of LG members, as well as their breakage mechanism in both heated and post-heated conditions, is not largely addressed in the literature. Few literature studies related to horizontal glass members combined experimental and Finite Element (FE) numerical calculations to reproduce the complex thermo-mechanical phenomena [45, 46]. The non-uniform temperature distribution within LG panels results in specific thermal boundaries and mechanical stresses that should be carefully considered in their analysis and design. An accurate prediction

of the actual temperature gradient is a key parameter for design. Also, changes in material properties due to fire exposure need to be accounted for [42].

The present research paper includes both original experiments on LG specimens and comparative calculations to study the above aspects. An experimental program is first discussed, in which a non-uniform thermal gradient is produced and then a traditional bending setup [38] is utilized to examine un-heated, heated, and heated & cooled LG specimens. A simplified analytical model [47] and more refined Finite Element (FE) numerical analysis utilizing ABAQUS [48] are then presented. The potentials and possible limits for both methods of analysis are discussed based on the experimental findings.

2. LG mechanical properties

Mechanical analysis of LG members depends on the composition of their layered sections [1, 2]. Given the viscoelastic characteristics of the interlayer, a multitude of research studies have been dedicated to the analysis of its mechanical properties and their effect on the overall structural capacity of the bonded glass panels. The flexural performance a typical LG panel, Figure 1a, is a function of the modulus of elasticity and shear modulus of the interlayer and the modulus of elasticity of the glass, which are affected by the temperature, as shown in Figures 1b and 1c. The shear modulus of the interlayer (G_{int}), which is a function of the operational temperature and the strain rate, greatly affects the behaviour and results in fully rigid, semi rigid, or independent behaviour of the glass panels, as shown in Figure 1a. A high number of experimental, analytical, and numerical investigations have been conducted to offer reliable material properties for PVB® and efficient calculation tools [49-52]. Having recognized that soda lime silica glass has a brittle elastic behaviour in tension and that the stiffness of bonding interlayer degrades with the increase of temperature, it is accepted to design LG based on the assumption that $G_{int} \rightarrow 0$ when the operational temperature is higher than 40 °C, thus, the LG section is treated as two uncoupled glass panels. Limited experimental efforts are available in the literature for LG components under temperatures higher than 60 °C.

The present research study addresses the shortage in the literature by experimentally examining the load-bearing performance of LG elements, which were subjected to non-uniform thermal gradients. The analytical and numerical studies account for thermo-mechanical modifications in the characteristics of interlayers and the rigidity of the glass.

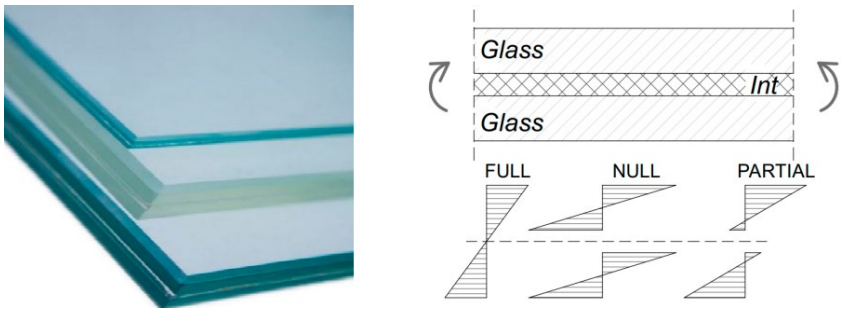

(a) Flexural stress distribution in LG section in case of full, null, and partial shear interaction

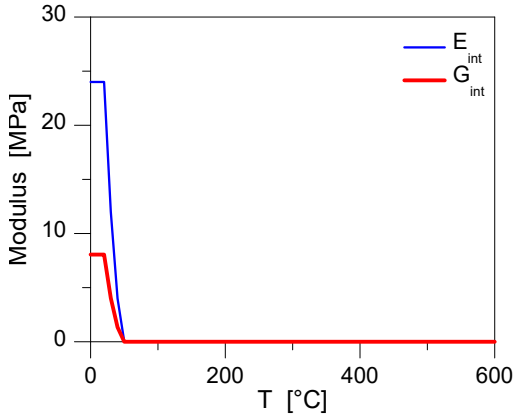

(b) PVB

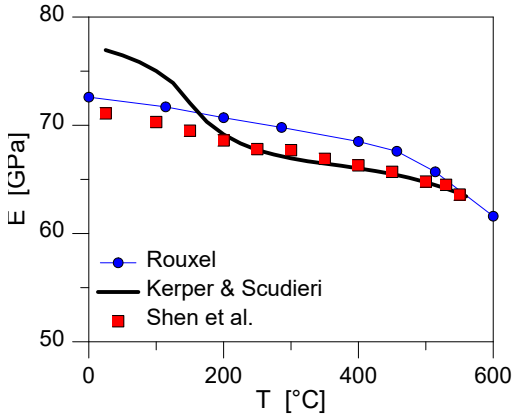

(c) Glass

Figure 1. LG flexural behaviour [34].

3. Experimental investigation

3.1 Non-uniform thermal exposure

Forty LG specimens were tested. Each specimen consisted of a composite section made up from two 5 mm thick annealed glass layers and a middle 0.76 mm thick PVB interlayer. The LG samples were manufactured by Safex* Hindustan glass work limited, Prayagraj, India. The nominal length (*L*), width (*B*), and thickness (*h*) of the samples were 172 mm, 40 mm, and 10.76 mm, respectively. As per the manufacturer, the glass composition was 74.00% SiO_2, 13.00% Na_2O, 10.50% CaO, 0.20% MgO, 1.30% Al_2O3, 0.30% K_2O, 0.20% SO2, 0.40% Fe_2O_3 and 0.10% TiO_2.

For the present study, a specialized test setup was constructed to allow exposing vertically installed LG samples to realistic fire situations [38]. The test apparatus, shown in Figure 2, was prepared using a cast iron burner and a set of aluminium plates, and can accommodate five LG samples simultaneously. The burner is located at the middle of the setup almost at the same elevation as the bottom of the vertically installed glass panels. The full experimental program was carried out in a laboratory facility with negligible influence of airflow. The LG samples were placed between the aluminium plates, which had a gap (t_{gap}) of 12 mm.

The forty LG specimens were divided into 4 groups, and each group was exposed to different fire duration (t_{exp} of 180, 360, 540, or up to 1200 seconds). The time-temperature relationships of the exposed (E) and unexposed (U) sides were recorded at the ten points, shown in Figure 3 (5 points per side), using J-type thermocouples and non-contact infrared thermometers.

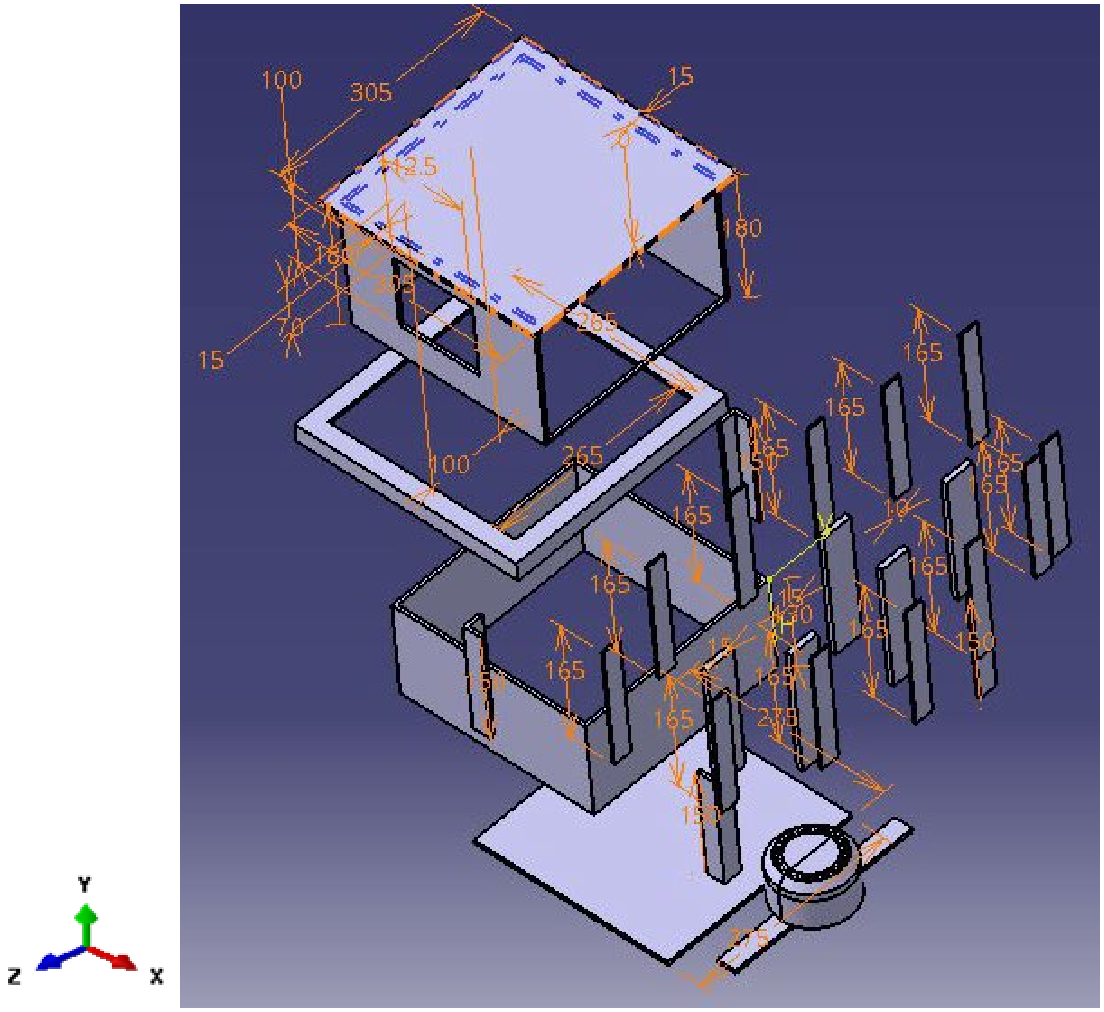

(a) Dimensions of different components of the test setup

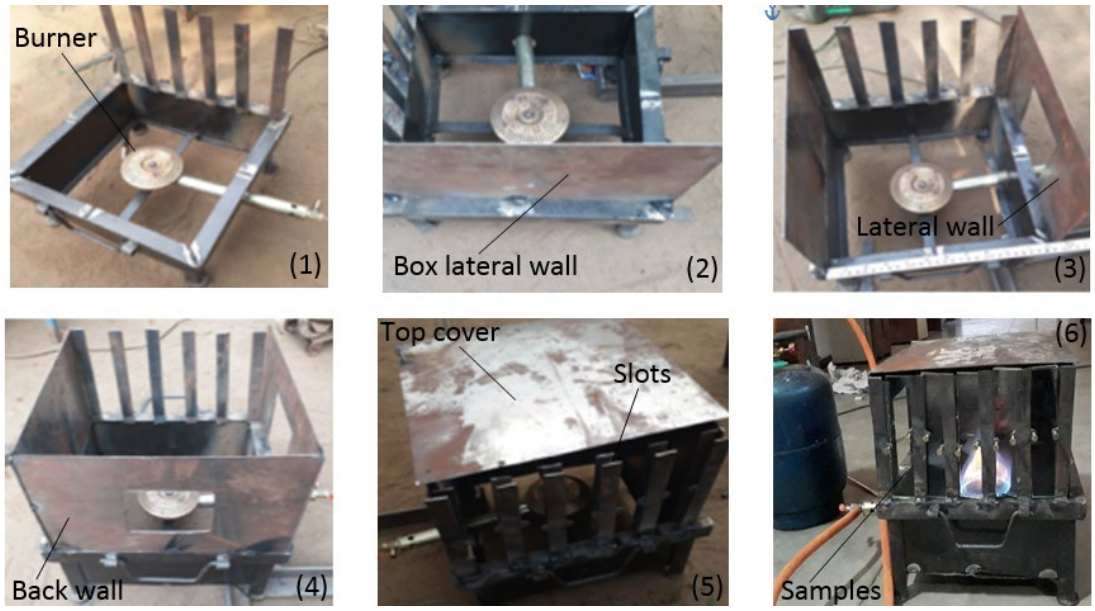

(b) Photos of the final setup

Figure 2. Experimental setup for LG specimens exposed to fire.

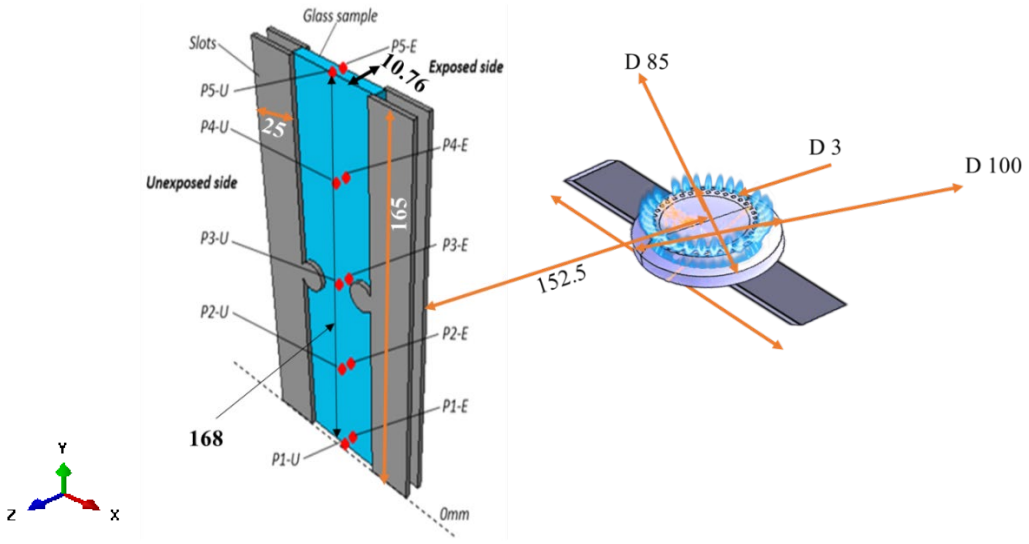

Figure 3. Schematic representation of reference control points for thermal measurements in LG specimens.

Figure 4 presents the measured variation of temperature with time for the tested LG specimens. The maximum and minimum recorded temperatures on both the exposed (E) and unexposed (U) sides are shown. The difference in temperature between the different samples considering the same point of measurement on E or U sides was less than 10 °C. Based on Figure 1 and from a mechanical point of view, the measured peak temperature, about 350°C, can be expected to correspond to a decrease of 5% in the modulus of elasticity *E* of glass and a full degradation of the shear rigidity of the PVB interlayer.

1

2

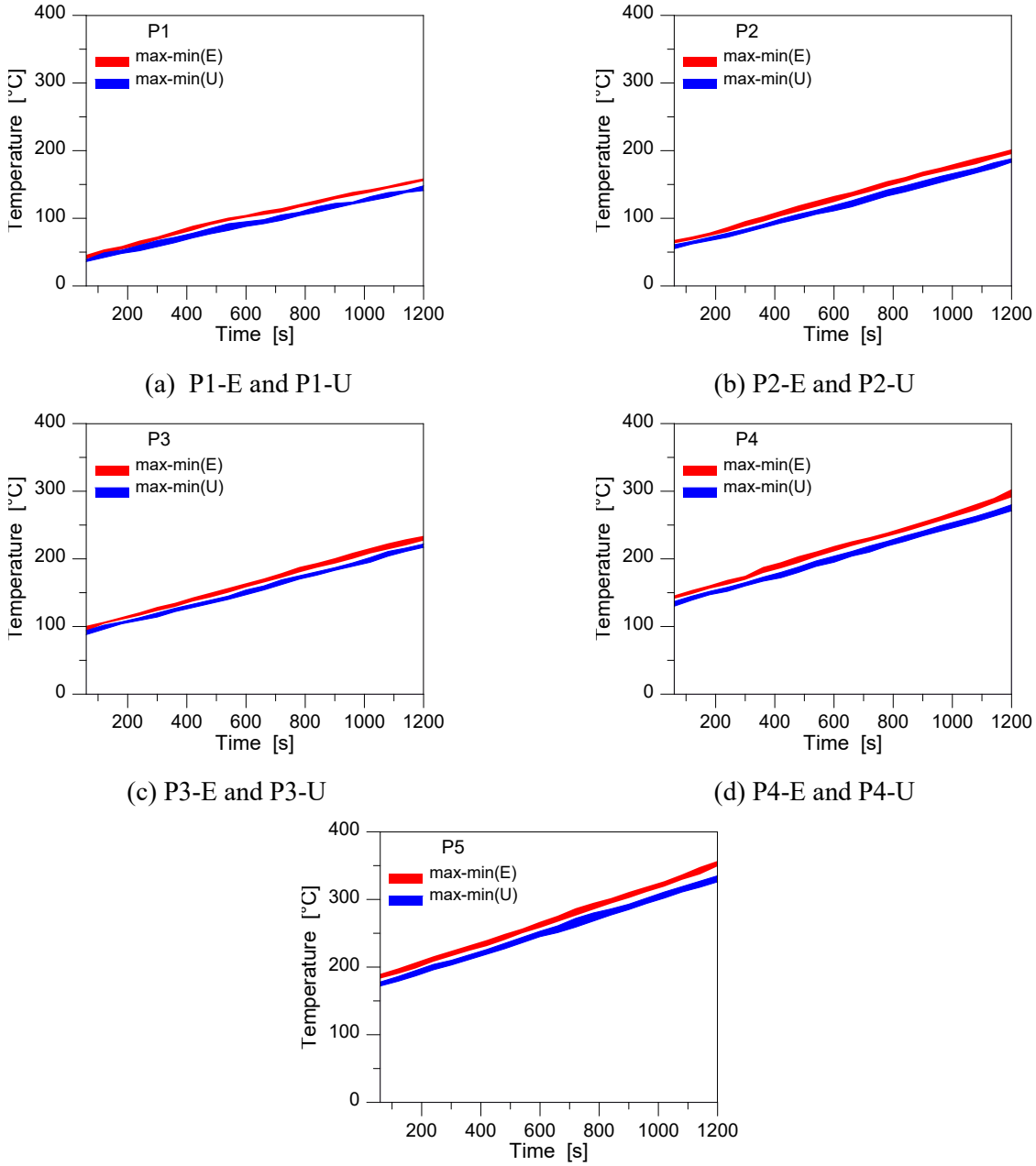

Figure 4. Time-temperature measurements for the tested LG specimens at different points on the exposed and unexposed surfaces.

Figures 5 and 6 show the variation of temperature along the height of the samples for the exposed and unexposed sides, while Figure 7 summarizes the overall gradient based on average measurements. The

distance z represents the distance from the base to the point of measurement, as shown in Figure 2. The maximum average temperatures of the E-side were 120 ºC, 205 ºC, 345 ºC and 360 ºC after t_{exp} of 180, 360, 540 and 1200 seconds, respectively. For the U-side, the maximum average temperature after 1200 seconds was 340 ºC. The temperature difference in Figure 7 reached 25 ºC near the top edge of the samples. The PVB layer was inspected after each fire test, and no visual damage was observed up to duration of 540 seconds. Post 540 seconds, the interlayer was found to start melting. Thus, the samples exposed to fire for 540 s has been chosen for the flexural tests. For duration of 1200 seconds, the PVB layer had completely melted.

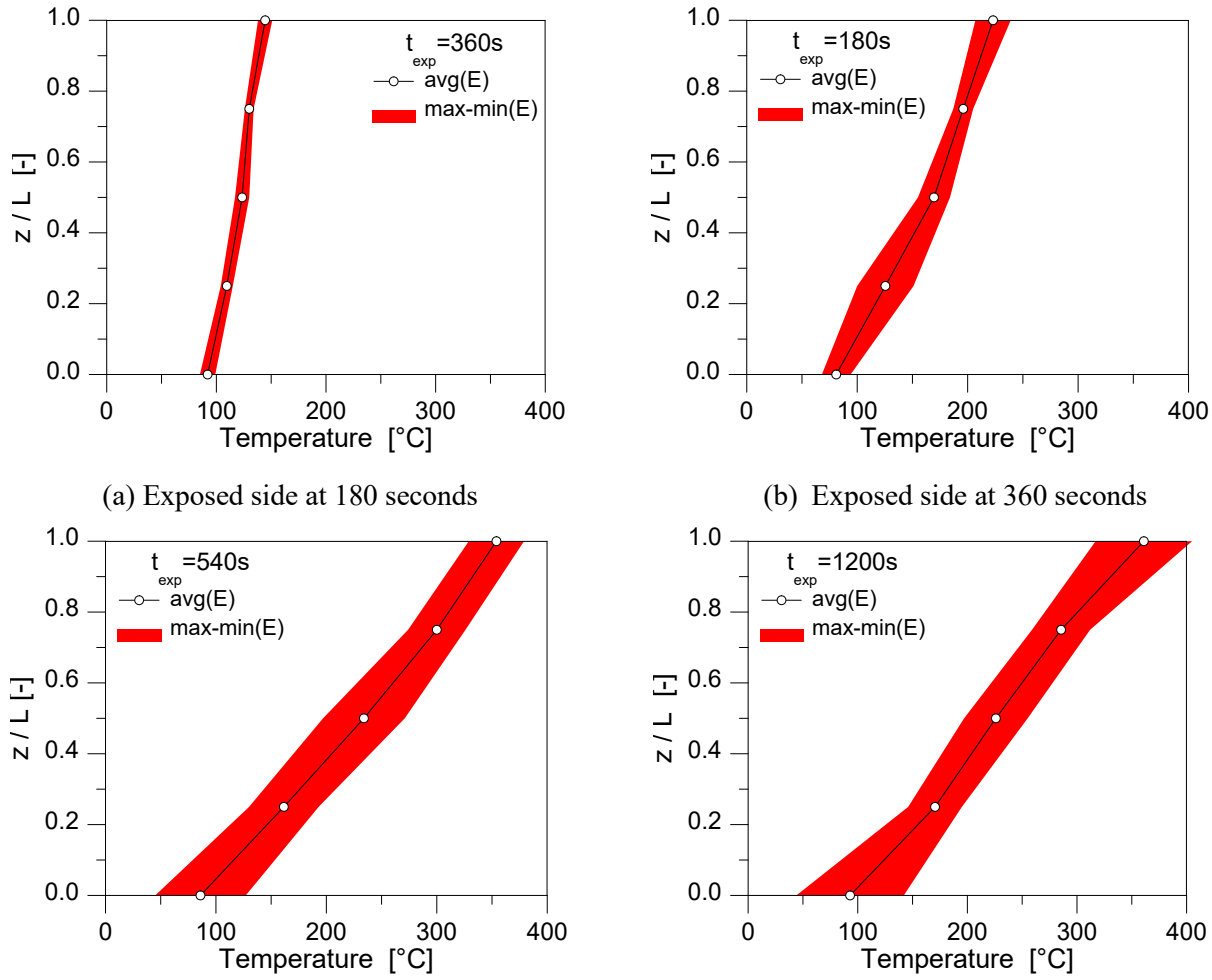

(a) Exposed side at 180 seconds

(b) Exposed side at 360 seconds

(c) Exposed side at 540 seconds

(d) Exposed side at 1200 seconds

Figure 5. Variation of the temperature of the exposed surface with the nondimensional height (z/L).

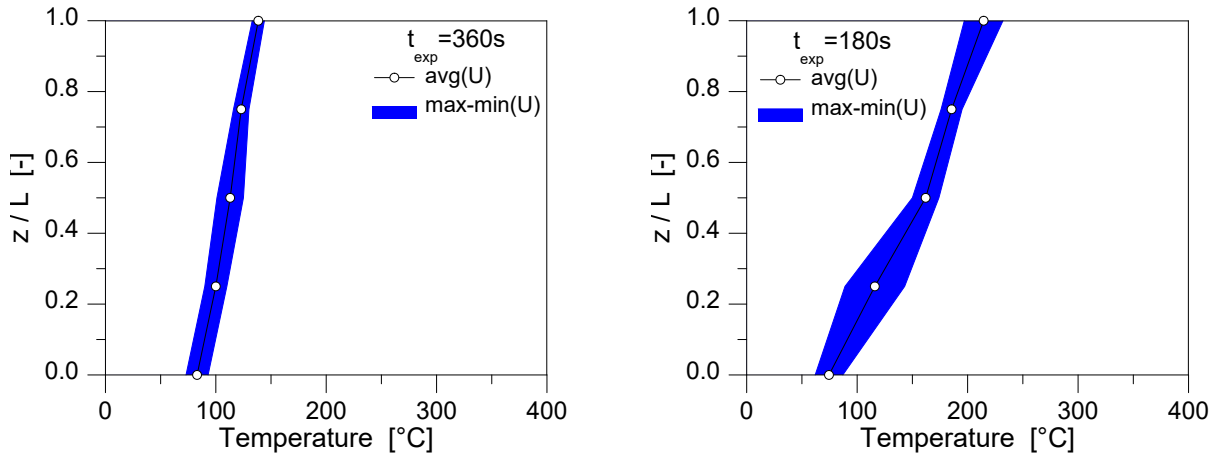

(a) Unexposed side at 180 seconds

(b) Unexposed side at 360 seconds

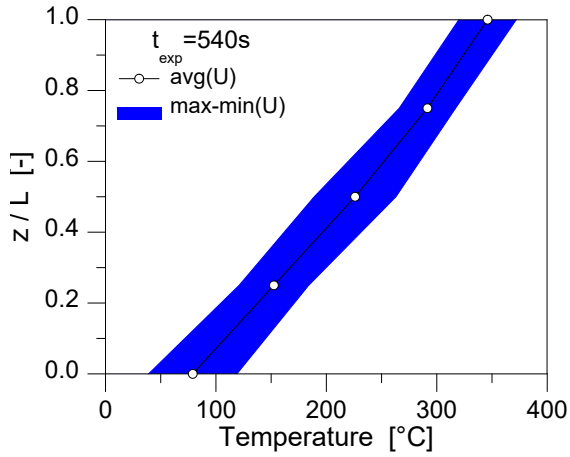

(c) Unexposed side at 540 seconds

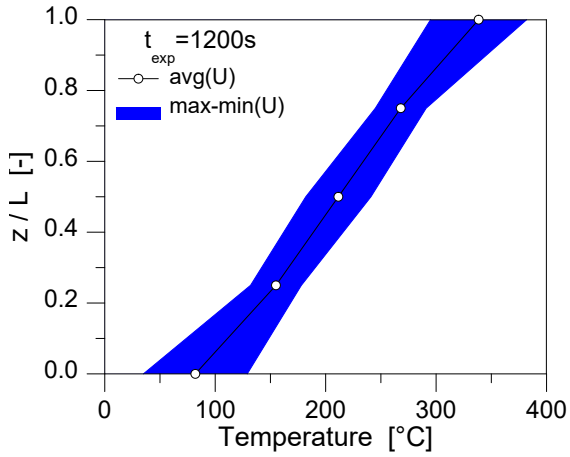

(d) Unexposed side at 1200 seconds

Figure 6. Variation of the temperature of the unexposed surface with the nondimensional height (z/L).

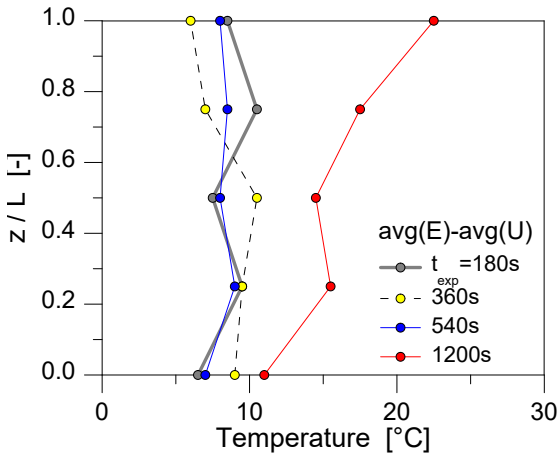

Figure 7. Measured temperature difference between the exposed and unexposed surfaces along the height of the LG specimens.

3.2 Flexural Tests

The experimental investigation followed the recommendations of ASTM D790-03 [38]. Flexural tests were performed on the fire-exposed LG samples as well as on five additional samples, which were not exposed to fire. The ten samples that were exposed to fire for a duration of t_{exp}=540 seconds were flexurally tested to capture the effect of the heated interlayer. The experimental setup is shown in Figure 8. The simple supports were positioned at 5 mm from the ends of the total span L. The load F was applied in a displacement-control protocol with a rate of 1 mm/min. The corresponding vertical deformation was recorded at the mid-span section of LG samples. The laboratory condition at the time of experiments was characterized by an average temperature of 28-31 °C.

Following the thermal stage in Section 3.1, the flexural tests were separately conducted on un-heated, heated & cooled down samples, and hot samples. The hot condition was achieved by moving the heated LG samples after fire exposure to the flexural machine in less than a minute. The heated & cooled LG samples were flexurally tested after 30 minutes from the end of the fire exposure, which allowed them to cool down to the room temperature.

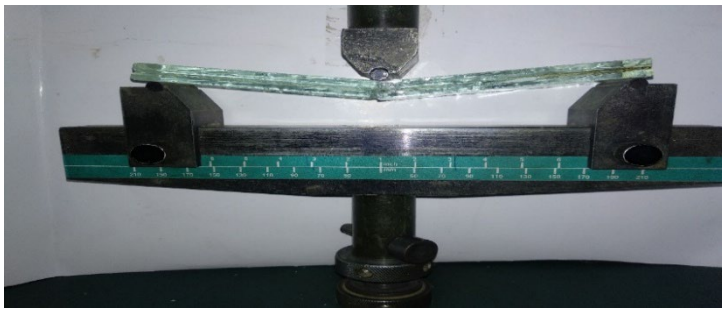

Figure 8. Three-point bending performance assessment of LG specimens.

The experimental force-displacement diagrams are shown in Figure 9, while the fracture patterns are shown in Figure 10. The duration needed to fracture the unheated glass samples was 1-3 minutes. For the heated samples, the duration reached 15 minutes due to the post-fracture residual ductility of the PVB.

The un-heated LG specimens cracked at a load of 280 to 574 N, which corresponded to a displacement of 1.2 to 2.4 mm. The post-cracking performance was not consistent among the test specimens, as specimens #3 and #4 failed at relatively lower loads. The fracture was characterized by multiple cracks distributed over a relatively wide fracture zone, Figure 10(a). Considering specimens heated & cooled (with t_{exp}= 540 seconds), their overall flexural performance was similar to the un-heated specimens. The load-bearing performance is shown in Figure 9(b). The fracture mechanism for heated & cooled specimens was found to affect a relatively smaller width of the total specimens, Figure 10(b). Specimens, which were tested while being hot,

showed a considerable deviation in the measured load-displacement behaviour, Figure 9(c). This behaviour can be attributed to the PVB interlayer, which was partially weakened during the heated stage and could not return to its normal condition before the flexural test. This resulted in a relatively lower interlayer shear transfer between the glass panels, and thus, an increased deformation for the tested specimens. Another possible explanation could be that the melted interlayer tends to close the glass cracks and prevent them from opening. Their peak load, 340 to 370 N, and the corresponding displacement, 1.4 to 1.6 mm, were similar to un-heated specimens. However, their fracture was reached at much higher displacement, which ranged between 11.5 to 11.8 mm. This performance can be useful in fire conditions as the glass panel can remain intact during fire for a longer period, which will prevent additional oxygen from supplying the fire, and thus, delay the flashover phenomenon.

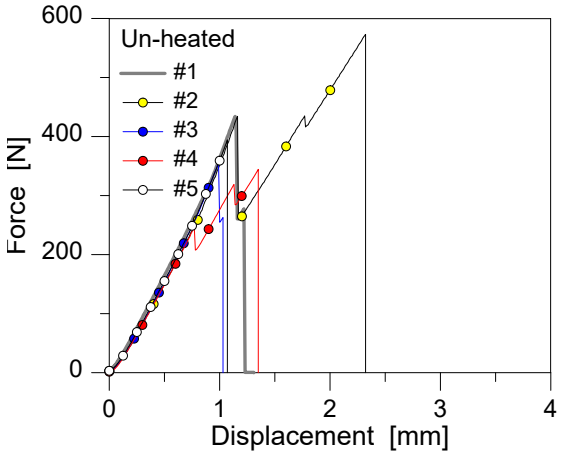

(a) Specimens unexposed to fire

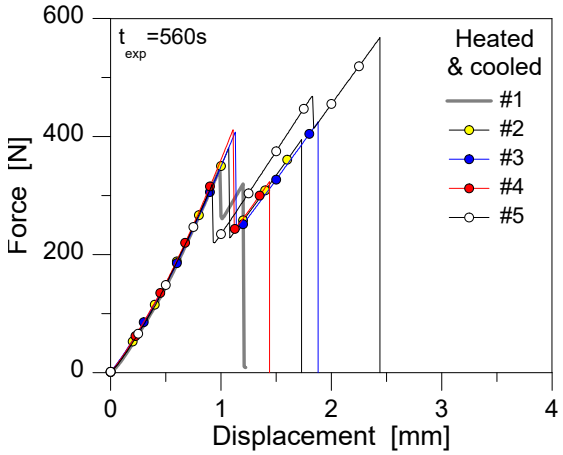

(b) Specimens exposed to fire and then cooled prior to flexural testing

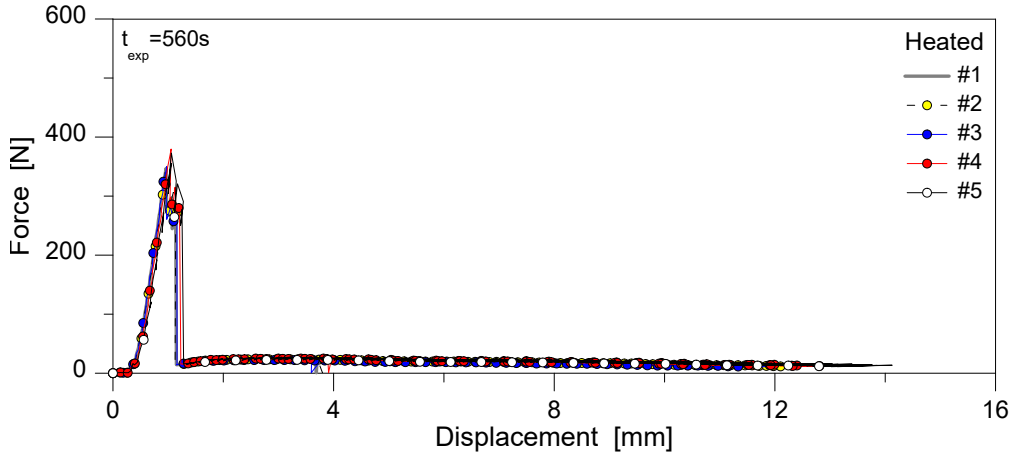

(c) Specimens exposed to fire and tested in flexural while being hot

Figure 9. Force-displacement curves from the bending setup.

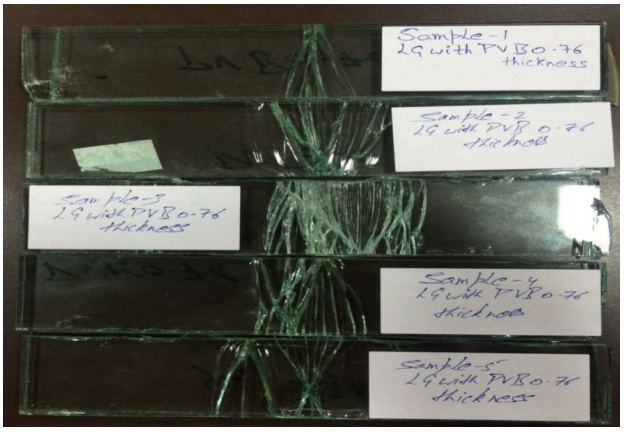

(a) Specimens unexposed to fire

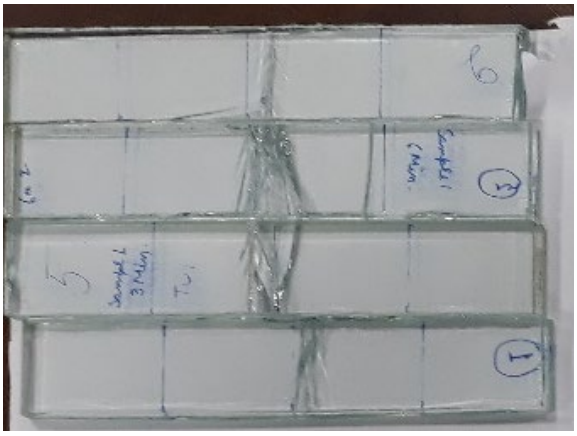

(b) Specimens exposed to fire and then cooled prior to flexural testing

(c) Specimens exposed to fire and tested in flexural while being hot

Figure 10. Fracture pattern of LG samples after flexural test.

From Figure 9, the mechanical performance of LG samples was assessed in terms of average fracture load, deflection at fracture, and bending stiffness. The results for the un-heated and heated & cooled specimens, Figure 11, are very similar. This finding confirms the relatively null residual effect of thermal exposure on the mechanical properties of glass. The specimens, which were flexurally tested while being hot, showed lower variability in the values of the failure load and much higher displacements at failure. The lower variability might be attributed to limited influence of microcracks/impurities of the glass and dominance of the properties of the softened interlayer in determining the flexural behavior. However, it is worth mentioning that average maximum load before fracture was lower in the heated condition, as the interlayer

was significantly affected at the boundaries of specimens, which played a significant role in determining the flexural strength. For the same reason, the higher displacement at failure for the heated condition was achieved because of the softened interlayer, which kept the fractured glass intact for longer duration.

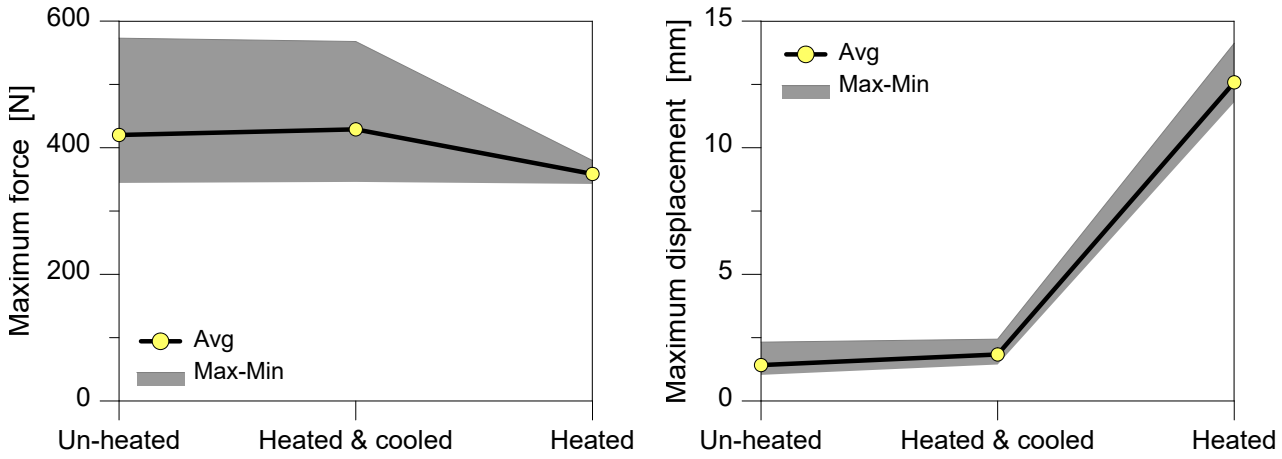

(a) Force (b) Displacement

Figure 11. Force and displacement for the LG specimens at collapse.

From the collected force-displacement records, the bending stiffness *EJ* of composite LG samples was also calculated. Experimental *EJ* values for the tested samples are summarized in Figure 12. The specimens, which were heated and then cooled prior to the flexural test, had a slight reduction in their stiffness of about 0.95%. The specimens, which were hot during the flexural test, showed a higher reduction of about 1.98%. Figure 12 clearly shows some variation between the *EJ* values within each group of samples, which reflects the variability of the value of G_{int} and *E* for glass under different thermal scenarios. It is also possible to notice that fire did not cause marked modification in the average bending stiffness *EJ*. The major effect was on the weak bond offered by PVB. This behaviour is further explained in Section 4.

Figure 12(d) shows in fact the overall variation of *EJ* with the imposed thermal condition. It can be perceived from average and min/max *EJ* estimates that specimens flexurally tested in hot conditions offered the lowest stiffness variability. The scatter of measured *EJ* values progressively increases for samples bended in cold conditions and suggests some further influence of *EJ* due to the viscous response of the interlayers at room temperature. For the heated & cooled samples, Figure 12(d), the average prediction is still in line with the un-heated samples, but again the max/min interval is minimized.

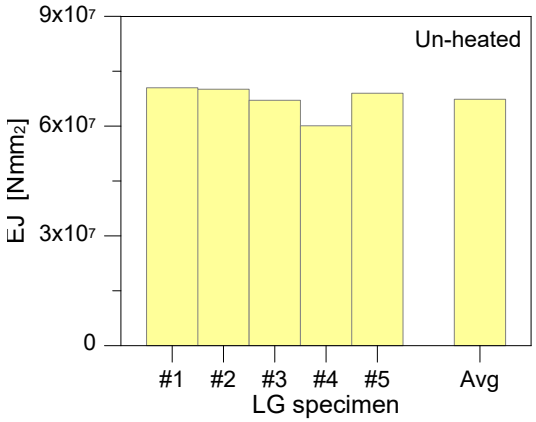

(a) Specimens unexposed to fire

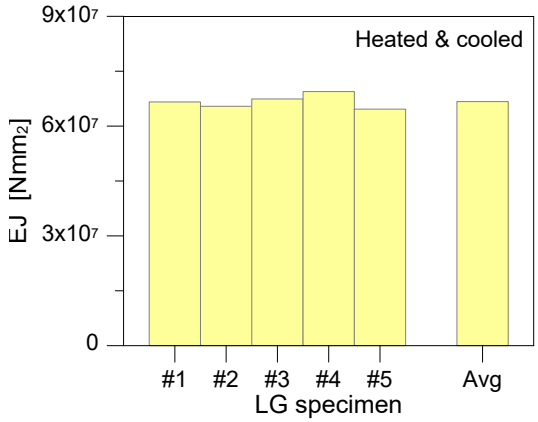

(b) Specimens exposed to fire and cooled prior to the flexural test

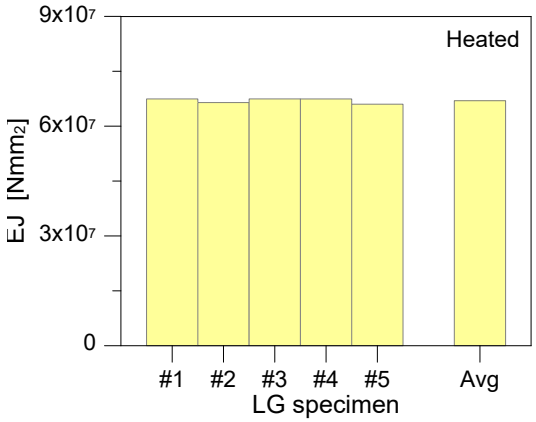

(c) Specimens exposed to fire and tested in flexure while being hot

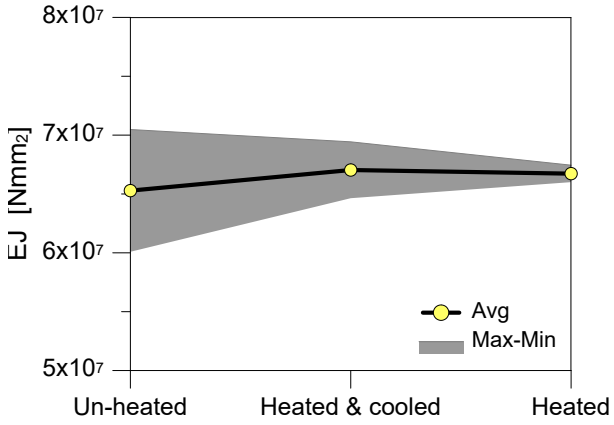

(d) Flexural stiffness comparison

Figure 12. Analytical flexural stiffness of LG specimens.

4. Analytical Investigation

4.1 Modelling

The application of the equivalent thickness (EET) approach to estimate the flexural stiffness is investigated in this section. For double LG panels, the equivalent thickness ($h_{ef,w}$) is estimated using Eq. (1) [39].

$$h_{ef,w} = \sqrt[3]{\frac{1}{\frac{\eta}{h_1^3+h_2^3+12I_s}+\frac{1-\eta}{h_1^3+h_2^3}}} \quad (1)$$

where $h_1$and h_2 are the thicknesses of glass layers (5 mm), h_{int} = 0.76 mm is the thickness of interlayer, I_s is the composite action effect evaluated using Eq. (2), and η denotes the shear bonding level and is given by Eq. (3). η ranges from 0 for weak connection to 1 for fully rigid connection.

$$I_s = \frac{h_1 h_2}{h_1 + h_2} \cdot [h_{int} + 0.5(h_1 + h_2)]^2 \quad (2)$$

$$\eta = \frac{1}{1 + \frac{E h_{int}}{G_{int} B} \cdot \frac{J_1 + J_2}{J_{tot}} \cdot \frac{A_1 A_2}{A_1 + A_2} \cdot \Psi} \quad (3)$$

In the above equations, E is the modulus of elasticity of glass, G_{int} is the secant shear modulus of the PVB interlayer (for the specific temperature and loading condition), B = 40 mm is the width of the panel, Ψ is a coefficient that accounts for the boundary conditions and load distribution [39] $= 10/L_0^2$ (with L_0= L – 5 mm ×2 = 162 mm, the actual bending span), J_i, A_i, and J_{tot} are given respectively by:

$$J_i = \frac{B h_i^3}{12} \quad (i = 1, 2) \quad (4)$$

$$A_i = B h_i \quad (i = 1, 2) \quad (5)$$

$$J_{tot} = J_1 + J_2 + \frac{A_1 A_2}{A_1 + A_2} \cdot [h_{int} + 0.5(h_1 + h_2)]^2 \quad (6)$$

The obtained equivalent thickness variation is shown in Figure 13 as a function of G_{int}. It can be seen that for an average room temperature of 28-30°C, the calculated $h_{ef,w}$ is very close to the lower "Abs" limit condition, due to the presence of a relatively weak bond (G_{int}≈ 4.5MPa the expected shear modulus based on Figure 1).

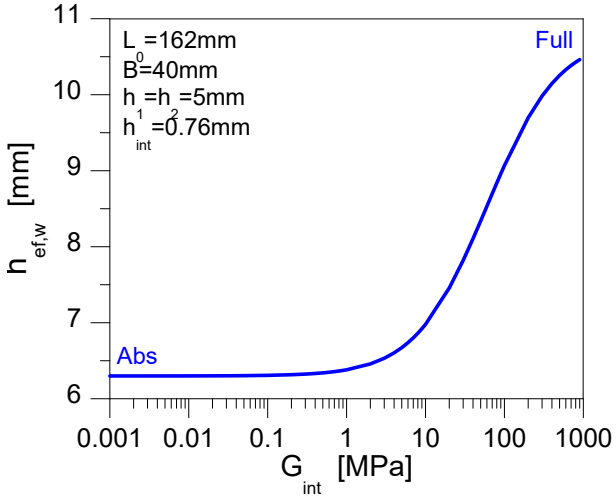

Figure 13. EET variation as a function of G_{int}.

4.2 Results and experimental comparison

For the analytical calculations carried out on the unheated samples, annealed glass was assumed to be temperature-independent and having a linear elastic stress-strain curve with E= 70 GPa. The initial composite bending stiffness EJ for the tested specimens was calculated analytically and compared to the

experimental results. The mid-span displacement f_{max} due to the imposed vertical force F was calculated using Eq. (7) and its variation is shown in Figure 14.

$$f_{max} = \frac{FL_0^3}{48EJ} \quad (7)$$

where $EJ = f(h_{ef,w})$.

For the un-heated LG samples, the interlayer was first assumed to provide a weak shear connection, with G_{int} of zero ("Abs" case). To ensure accurate analytical solutions, it is needed to account for the loading scenario, temperature, humidity, thickness of constituent layers, and the PVB properties. These factors cannot be realistically estimated for different LG samples; thus, it seems adequate to use a weak bond condition for the interlayer and nominal thicknesses for all the LG components. For comparisons, analytical calculations are also repeated with a rigid shear connection in which G_{int} approaches the shear rigidity of glass, "Full" case in Figure 14, and an intermediate case, with G_{int}= 4.5 MPa, was also considered.

The resulting analytical flexural responses, shown in Figure 14, and their comparison to the five tested samples clearly indicate that the weak bonding condition provides a good estimate for the initial stiffness of tested LG specimens. Minor deviation can be seen for cases of G_{int}= 4.5 MPa and zero, which can be due to the modified interlayer properties, as well as the minor deviation of the real thickness from the nominal values. Regardless, the analytical model can correctly reproduce the elastic flexural response of un-heated LG samples at ambient temperatures. It should be noted that the model suggested in [55] can be modified to analyze bending behaviour of cracked LGs.

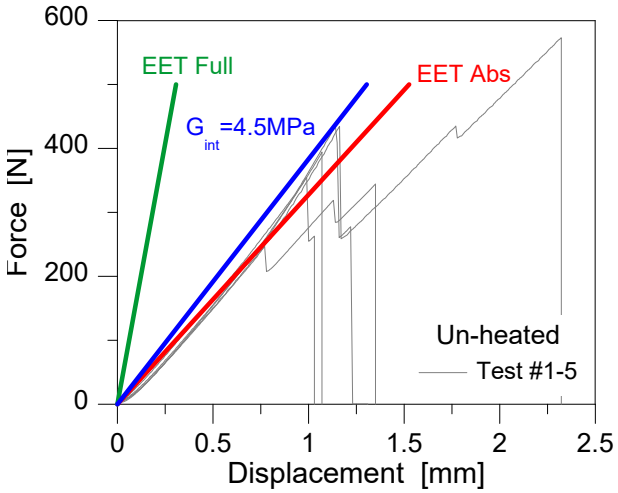

Figure 14. Flexural response of un-heated LG specimens.

The same analytical model and procedure was then examined for LG samples subjected to thermal cycles. Following the preliminary un-heated calculations in Figure 14, a weak "Abs" shear connection was again assumed to represent the PVB foils. For this calculation step, the LG panel is assumed to have to a uniform temperature. This approach represents a lower limit condition for the examined LG samples, given that the temperature evolution is typically non-uniform (as in Section 3), and thus the corresponding degradation of material properties (i.e. Figure 1) is also non-uniform. The effect of temperature on the glass panel was taken into consideration using the experimental E values, given in Figure 1. For an imposed uniform temperature, the modified E value is estimated from Figure 1, and then $h_{eq,w}$ is estimated using Eq. (1). Because of the variation of the temperature with time, the material properties change, and calculations based on Eq. (1) need to be repeated. In this manner, it is possible to predict the bending stiffness EJ of the heated LG sample, and its modification with thermal boundaries. The resulting EJ values are shown using the blue curve in Figure 15. Due to the assumptions of uniform temperature within the LG section, a significant reduction in the EJ value can be observed at about 100 °C (-12%). For higher imposed temperatures, the EJ degradation is still linear but less pronounced than in the first 100°C. A -18% reduction is predicted at a temperature of 400°C.

For comparisons, the experimental (average) EJ values are also presented in Figure 15. It is clear that the adapted EET analytical model is able to predict the EJ values for the un-heated and the cooled-down samples, with reasonable accuracy. This is due to the negligible thermal effects of the relatively high but short-term fire exposure (t_{exp}= 540 s). However, for the heated samples, the predicted EJ value in Figure 15 is 10% lower than the corresponding experimental results. This lower estimate can be attributed to the uniform temperature assumption in LG, or the used E values for the glass [34, 35].

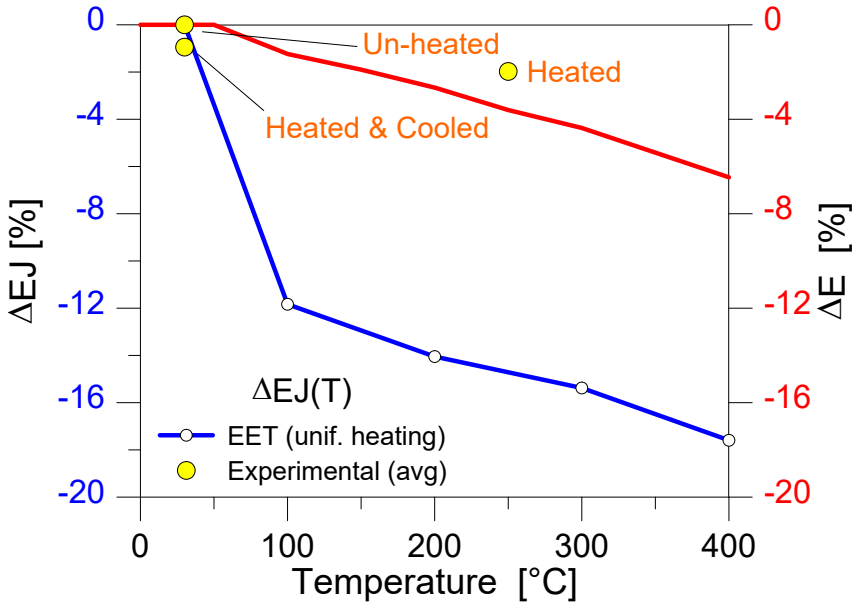

Figure 15. Expected analytical flexural stiffness variation with temperature for the tested LG specimens.

5. Numerical Investigation

5.1. Modelling of heated specimens

The tested specimens were modeled using ABAQUS software like in a previous research step of the project [30], in which a similar test setup was used for monolithic samples in place of LG specimens. The analysis was composed of a thermal stage (s1) to impose the experimental temperature scenario (heating stage), followed by a coupled static stage (s2) to calculate the thermal stresses in the burner setup due to temperature variation, and another mechanical loading stage (s3) to examine the flexural behaviour. The adopted general procedure of simulation is summarized in Figure 16. The thermal variation effect of metal slots in stages s1 and s2 was disregarded, based on earlier studies [30]. Besides, variations with temperature in the mechanical properties of the different materials were considered.

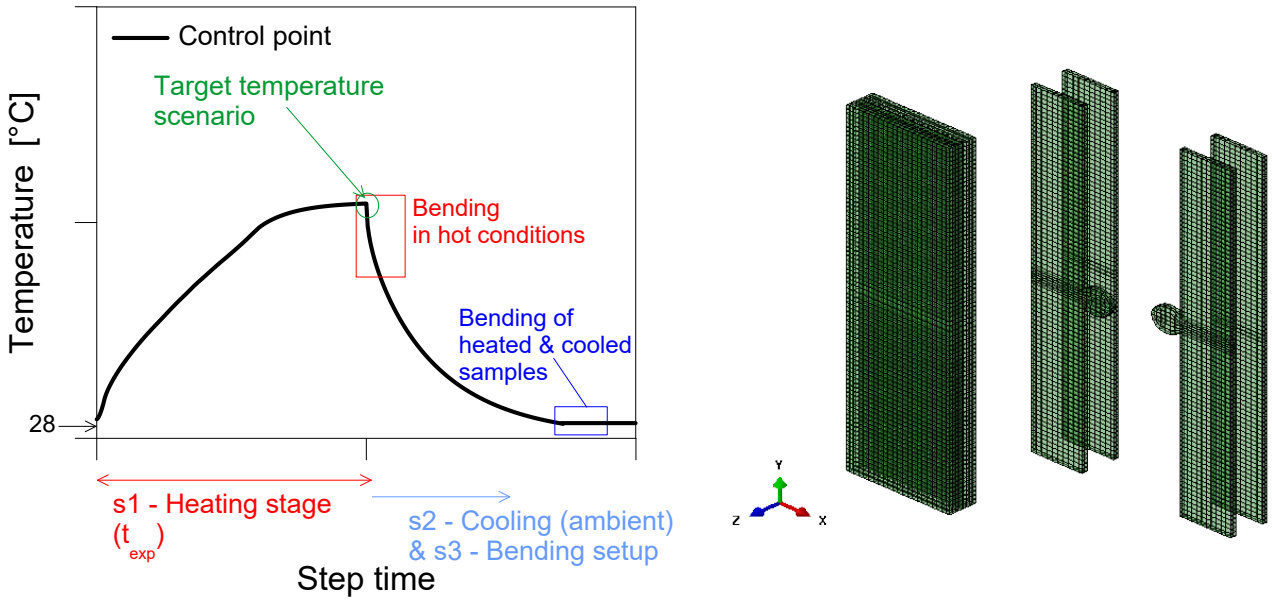

Figure 16. (a) Schematic procedure for thermal and mechanical FE numerical analysis of LG samples under different thermal cycles and (b) mesh detail.

The thermo-mechanical FE model followed the literature and the experimentally validated models for monolithic and LG members [35, 36, 37]. In the present study, the thermal simulation represented stage s1. The reference glass specimen was supported at its bottom surface and kept in vertical position by lateral metal slots as in Figure 3. At the end of stage s1, the glass specimen was placed in horizontal position with end supports for bending and / or cooling. This experimental sequence required a series of modifications in thermo-mechanical details of the FE assembly, to account for realistic boundaries through the uncoupled thermal and mechanical simulation stages. The glass panels, PVB interlayer, and metal slots were first

modeled in their nominal geometry using DC3D8 brick elements for the full thermal analysis (s1 to s3 steps). A regular mesh pattern with 2 mm average edge size and 4 solid elements in the thickness of each glass layers (2 in the thickness of PVB) was used. A total of 16,236 bricks for LG and 7,026 bricks for the metal parts (103,842 DOFs in total) were used. The final layout is shown in Figure 16(b).

A rigid temperature-independent connection was utilized at the interface of the glass and PVB layers. This means that possible delamination effects were disregarded, but material degradation with temperature was only considered. The thermo-physical and mechanical characterization of glass are shown in Figure 17, which were utilized by Kozłowski and Bedon [35]. The moduli of glass and PVB were assumed to follow the modifications presented in Figures 1(b) and 1(c). Temperature-independent material properties were indeed used for the metal slots [30].

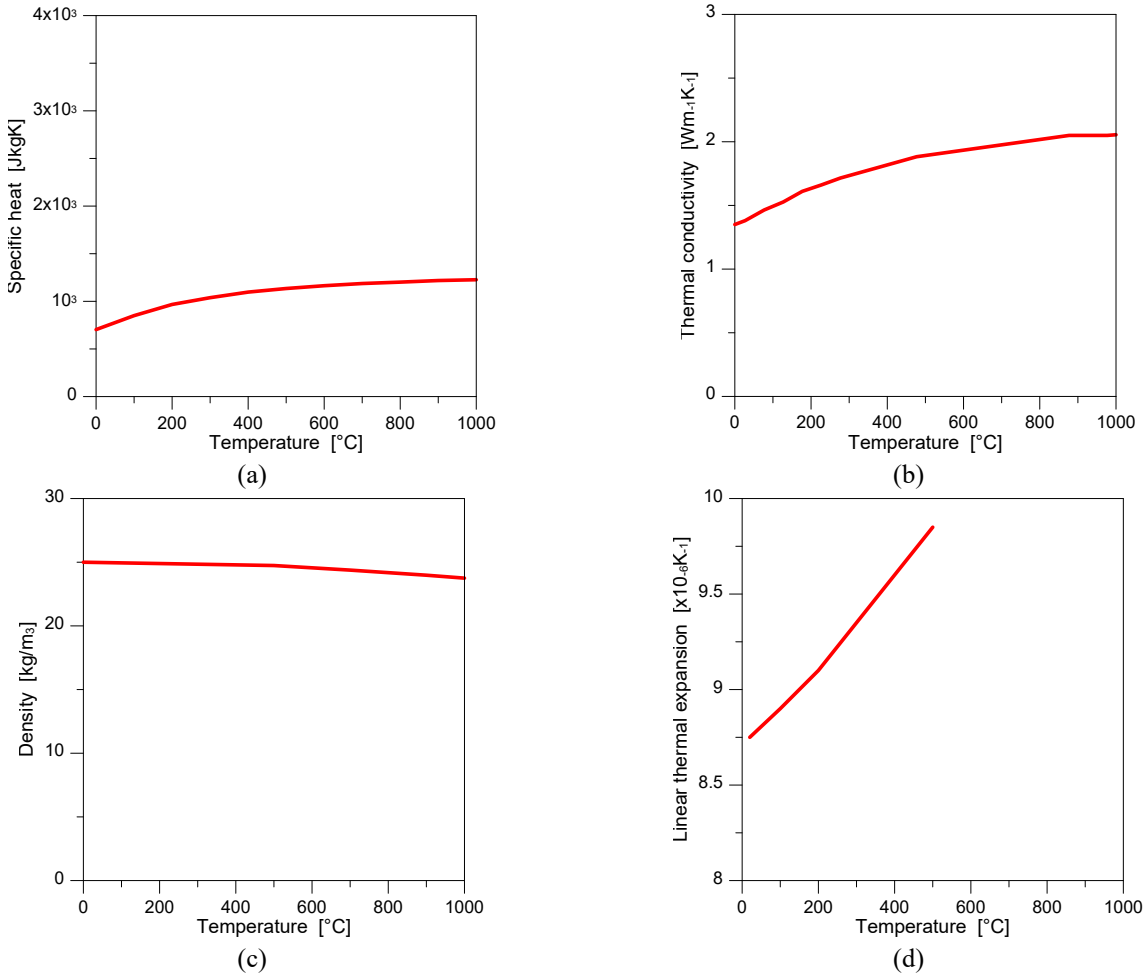

Figure 17. Selected glass material properties:
(a) specific heat; (b) thermal conductivity; (c) density; (d) thermal expansion coefficient.

For the heating thermal stage (s1), the input experimental temperatures of the 10 controls points in Figure 3 were taken into account over an exposure time of t_{exp}= 540 seconds. To reproduce the real non-uniform thermal boundaries. These measured temperatures were imposed to both the E and U surfaces of glass. After the fire exposure in s1, the FE assembly was moved to the mechanical stage to capture thermal stresses in the components. The bending loading stage was then carried out for the simply supported LG samples, either in hot conditions (s2) or at room temperature after cooling (s3). Cooling was assumed to take place in the same simply supported bending setup.

In both cases, the uncoupled mechanical analysis was carried out replacing the original brick components of glass and PVB with C3D8R elements, having identical mesh pattern as in the thermal model (Figure 16b). The temperature-independent metal parts were only considered in the mechanical stage s1 to account for the potential thermal stresses at the edges of glass. The metal parts were then physically deleted from the FE assembly and replaced by nodal boundaries to reproduce the setup shown in Figure 8. In such a procedure, the temperature nodal records and evolutions in glass and PVB from stage s1 (and / or s2) were used in the bending stage (s2 or s3) to account for the non-uniform thermal exposure of heated or heated & cooled specimens, respectively.

In doing so, for both stages s2 and s3, no experimental temperatures were imposed to the heated models after stage s1. Cooling / bending was thermally simulated assuming an average laboratory temperature of 28 °C. The heat transfer boundary conditions for radiation and convection were, thus, defined as incident radiation from a black body [35]. Following [53, 54], the heat transfer coefficient was set to 25 W/m^{2}K for the glass surface and 8.02 W/m^{2}K for the unexposed surfaces. A standard emissivity coefficient equal to 0.95 was used [53].

5.2. Results

Following the previous experimental and analytical discussions, major attention is spent in the present section for specimens bended under hot conditions (s2). Given that the heated LG specimens were tested flexurally immediately after the fire exposure (s1), no intermediate cooling effects were considered for FE modelling.

The FE results in Figure 18 represent the time instant at which the LG samples are removed from the burner. Figure 18(a) shows the contour plot of imposed temperatures for the unexposed side after t_{exp} of 540 seconds, while Figure 18(b) summarizes the typical temperature evolution at the 10 control points of the FE assembly for the E and U sides of the glass panel. The simplified FE procedure is clearly able to match the experimental scenario. The temperature and thermal stresses for PVB are shown in Figures 18(c) and (d). The PVB temperature is found to be of the same order of magnitude as the E and U sides of glass panels. The peal local stresses, observed in Fig. 18(d), are similar to the experimental observations, shown in Figure

10(c). The top glass panel experienced the highest temperatures, and thus major stress concentrations, as shown in Figure 18(e). The maximum principal stresses were numerically measured as 19 MPa.

For the mechanical loading stage, the boundary conditions matched those of the experimental setup. The effect of the fire exposure was reflected in the input temperature-dependent mechanical properties of glass and interlayer materials, as well as by the residual thermal stresses in Figure 18.

Figure 19 shows the typical bending response. While point A marks the area that experienced the highest temperature in the heating stage, point B corresponds to the maximum tensile stress during the mechanical loading stage. The mechanical loading stage, see Figure 19(a), followed the t_{exp} phase and included the ambient cooling of materials while loading. The force-displacement response is shown in Figure 19(b), which roughly captures the experimental observations but still to lack the local effects happening due to the changes in the PVB properties. Figure 19(c) shows that the fracture initiation is expected to initiate at the mid-span region of glass panels. The inverse analysis of fracture stresses at the edge suggests a material strength in the order of 20 MPa. Given the presence of a mostly melted PVB interlayer, the same order of magnitude of maximum stresses can be perceived for both glass panels, as shown in Figure 19(d). Such a stress magnitude is significantly lower than the nominal tensile bending strength of annealed glass (45 MPa the characteristic value in cold conditions). At the same time, the estimated stress is in good correlation with thermal shock resistance values of literature for glass specimens. The average experimental thermal failure is in the order of 15 MPa as reported in [42].

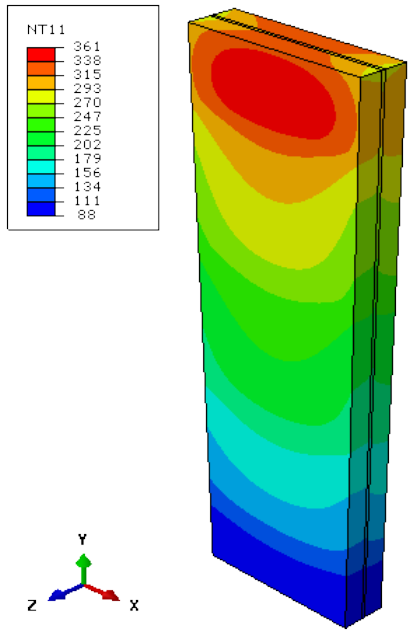

(a) Temperature in glass

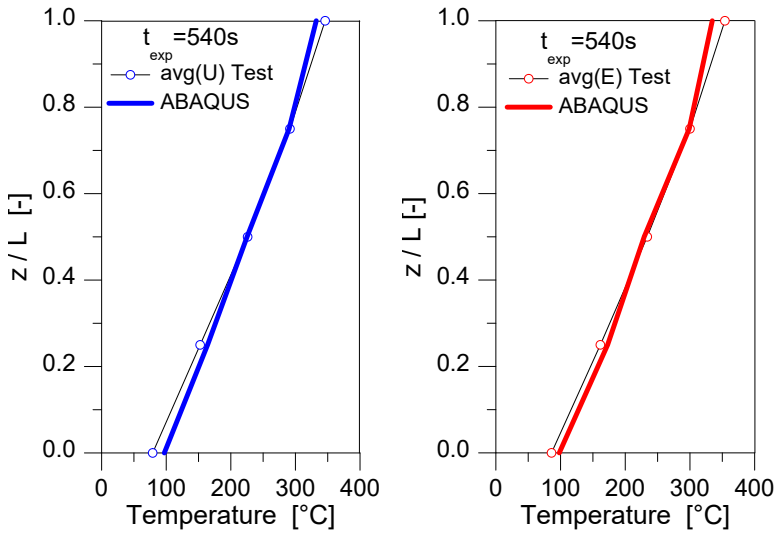

(b) Temperature at selected control points (U and E sides)

at t_{exp}= 540 s (U side)

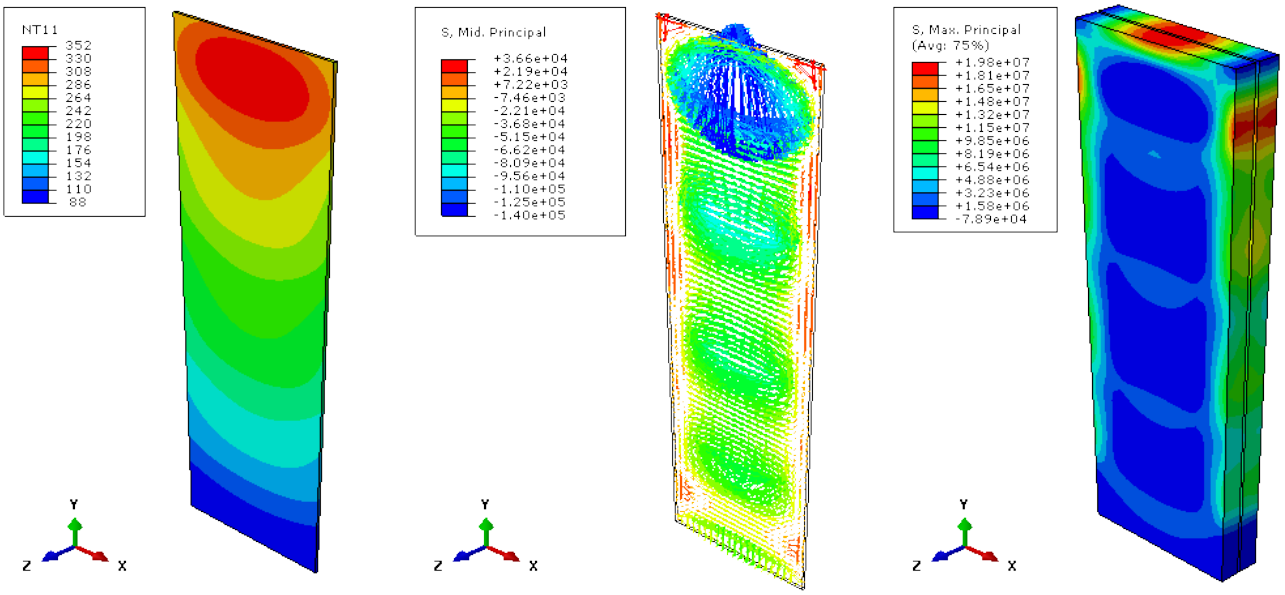

(c) Temperature in PVB at t_{exp}= 540 s (U side)

(d) Thermal stresses in PVB at t_{exp}= 540 s (U side)

(e) Thermal stresses in glass at t_{exp}= 540 s (U side)

Figure 18. Numerical thermal analysis of LG specimens (legend values in °C and Pa).

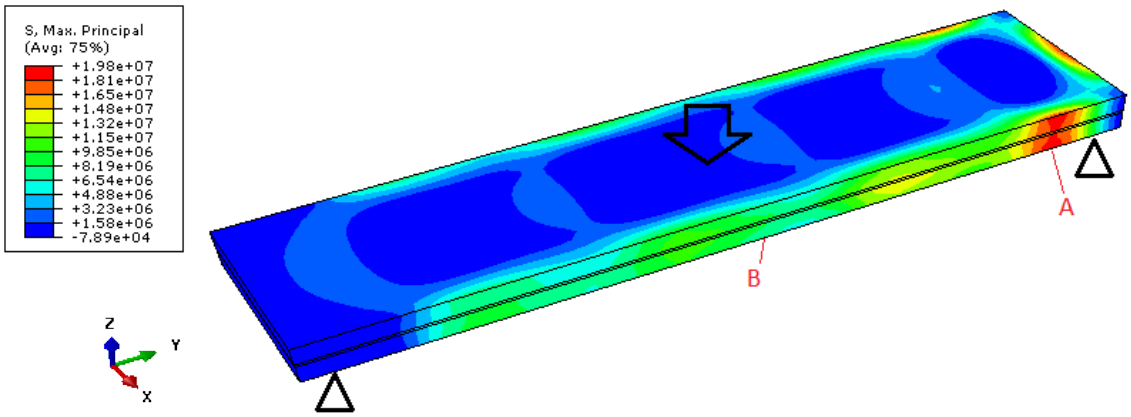

(a) Starting configuration for bending setup (from t_{exp}= 540 s)

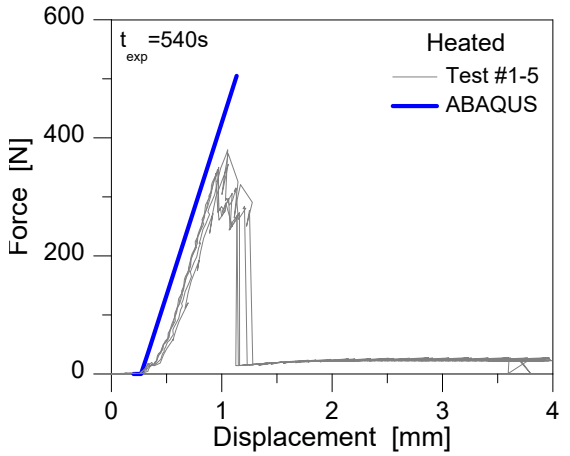

(b) Force-displacement response

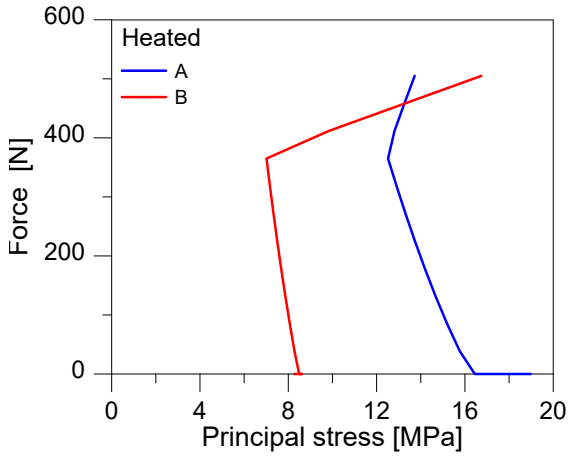

(c) Force-stress response at points A and B

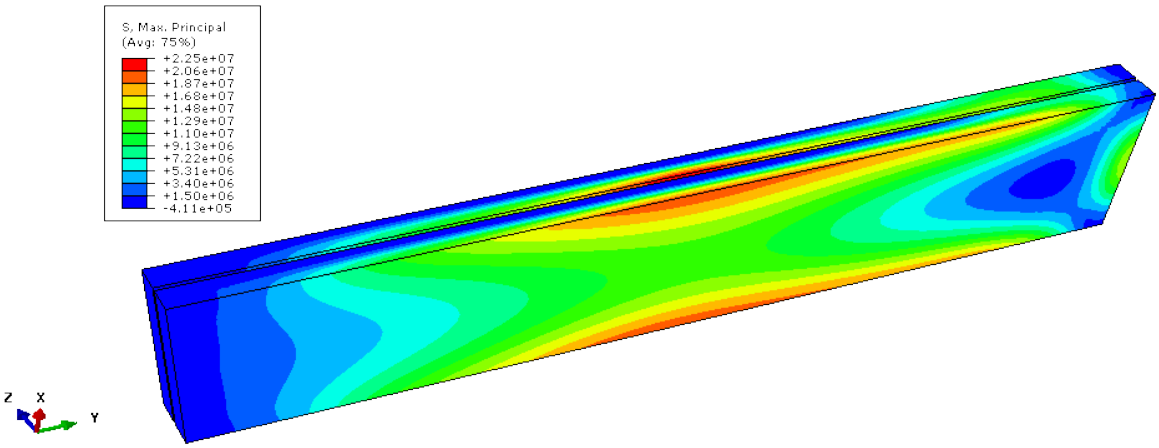

(d) Contour plot of maximum principal stresses at Force of 500N (bottom view)

Figure 19. Bending performance of the heated LG specimens (legend values in Pa).

6. Conclusions

This manuscript reports out-of-plane bending behaviour of laminated glass (LG) members exposed to fire, based on experimental, analytical, and numerical approaches. Attention was focused on the different thermal boundaries (non-uniform thermal exposure) and thermal histories, and their effects on the actual mechanical performance of LG element in out-of-plane bending. The conclusions of this study can be summarized in the following points.

- The out-of-plane bending performance of LG members was not affected by exposure to temperatures up to 400 °C, when they were mechanically tested after being cooled down.
- The small variation in the pre-cracked flexural stiffness of the tested specimens under different thermal histories confirms the stability of thermo-physical and mechanical properties.
- During flexural tests, fracture was found to initiate in the lower glass plate near the mid-span section (load application), and then to move to the upper glass plate.
- The un-heated LG samples generally experienced multiple fractures during the flexural test and were thus characterized by a wider cracked zone at collapse.
- The bending collapse for both the un-heated and heated & cooled LG specimens was mostly characterized by an abrupt failure mechanism, without any kind of residual stiffness nor ductility.
- The heated LG samples which were tested flexurally in hot conditions proved to offer residual capacity in out-of-plane bending with deformations reaching ten times the other specimens. This response is due to the melted interlayer, which allowed the glass panels to stay intact during the flexural test. The pre-cracked bending stiffness of the LG specimens, furthermore, does not suggest relevant modifications in the modulus of elasticity of glass.
- Both the analytical and numerical analyses confirmed the relevant effects of non-uniform temperature conditions on the LG specimens.
- In the case of un-heated and heated & cooled specimens, the calculations were found to mostly agree with the load-deflection and bending stiffness experimental data, and to confirm the presence of a rather weak bonding connection between the glass layers.
- For the heated LG samples bended in hot conditions, major limits were observed in the analytical and numerical models to capture the progressive modification of material properties with temperature modification.

Acknowledgments

The present research study is financially supported by the Department of Science and Technology, India, and IC Impacts, Canada (Grant: DST/INT/CANADA/IC-IMPACTS/P-11/2019/G) and by Invertis University, Bareilly (UP), India.

Data availability

Data will be made available upon request.

References

[1] M Haldimann, A Luible, M Overend (2008). Structural use of glass. IABSE, Zurich (CH), ISBN 978-3-85748-119-2

[2] JD Musgraves, J Hu, L Calvez (2019). Springer Handbook of Glass, https://doi.org/10.1007/978-3-319-93728-1

[3] Galuppi and Royer-Carfagni. Composites Part B: Engineering 64 (2014): 202-213.

[4] Pelayo and López Aenlle. Journal of Sandwich Structures & Materials 21.2 (2019): 439-463

[5] A Vedrtnam (2019). Novel treatment methods for improving fatigue behavior of laminated glass. Composite Part B, 167:180-198, doi: 10.1016/j.compositesb.2018.12.037

[6] Lopez Aenlle and Pelayo. Applied Mechanics Reviews 65.2 (2013).

[7] Marcon et al. Engineering Fracture Mechanics 127 (2014): 71-82.

[8] J Hänig, P Bukieda, M Engelmann, I Stelzer, B Weller (2019). Examination of Laminated Glass with Stiff Interlayers – Numerical and Experimental Research. International Journal of Structural Glass and Advanced Materials Research, 3(1): 1-14, doi: 10.3844/sgamrsp.2019.1.14

[9] A Vedrtnam, SJ Pawar (2019). Experimental and Simulation Studies on Bending Behavior of Laminated Glass with Polyvinyl Butyral and Ethyl Vinyl Acetate Inter-layers of Different Critical Thicknesses. Journal of Sandwich Structures and Materials, doi: 10.1177/1099636219830143

[10] Galuppi and Royer-Carfagni. Composites Part B: Engineering 147 (2018): 227-239.

[11] Biolzi, Cattaneo, Rosati. Construct Build Mater 2010;24(4):577-84.

[12] Biolzi et al. Compos Struct 2016;157:337-47.

[13] Castori, Speranzini. Compos B Eng 2017; 125:89-99.

[14] M Martín, X Centelles, A Solé, C Barrenechec, AI Fernández, LF Cabeza (2020). Polymeric interlayer materials for laminated glass: A review. Construction and Building Materials, 230, 116897

[15] S Huo, H Reis (2008). Estimation of adhesive bond strength in laminated safety glass using guided mechanical waves: Part I. An energy velocity approach. Insight, 50(3): 146-152, doi: 10.1784/insi.2008.50.3.146

[16] A Vedrtnam (2018). Experimental and simulation studies on delamination strength of Laminated Glass having Polyvinyl Butyral and Ethyl Vinyl Acetate Inter-layers of Different Critical Thicknesses. Defense Technology, 14(4): 313-317

[17] C Bedon (2019). Issues on the vibration analysis of in-service laminated glass structures: analytical, experimental and numerical investigations on delaminated beams. Applied Sciences, 9(18): 3928

[18] D Wei, D Li, Z Zhang (2019). Simulation Study of Low-Velocity Impact on Polyvinyl Butyral Laminated Glass Based on the Combined TCK-JH2 Model. Applied Sciences, 9(15), 3204, doi: 10.3390/app9153204

[19] K Osnes, S Dey, OS Hopperstad, et al. (2019). On the Dynamic Response of Laminated Glass Exposed to Impact Before Blast Loading. Experimental Mechanics, 59: 1033–1046

[20] L Figuli, D Papan, Z Papanova, C Bedon (2021). Experimental mechanical analysis of traditional in-service glass windows subjected to dynamic tests and hard body impact. Smart Structures and Systems 27 (2), 365

[21] M Larcher, G Solomos, F Casadei, N Gebbeken N (2012). Experimental and numerical investigations of laminated glass subjected to blast loading. Int J Impact Eng, 39(1): 42–50

[22] X Zhang, H Hao, G Ma (2013). Laboratory test and numerical simulation of laminated glass window vulnerability to debris impact. Int. J. Impact Eng., 55: 49–62

[23] M Förch (2020). Time-Temperature Dependency of Laminated Glass Subjected to Blast Load – A Numerical Study. International Journal of Structural Glass and Advanced Materials Research, 4(1), 69-81, https://doi.org/10.3844/sgamrsp.2020.69.81

[24] C Butchart, M Overend (2013). Influence of Moisture on the Post-fracture Performance of Laminated Glass, Glass performance days, pp. 59–61

[25] G D'Ambrosio, L Galuppi, G Royer-Carfagni (2019). Post-breakage in-plane stiffness of laminated glass: an engineering approach. Glass Structures & Engineering. doi: 10.1007/s40940-019-00099-1

[26] X Wang, J Yang, W Tung A Chong, P Qiao, S Peng, X Huang (2020). Post-fracture performance of laminated glass panels under consecutive hard body impacts, Composite Structures, 112777, doi: 10.1016/j.compstruct.2020.112777

[27] P Pagni (2002). Thermal glass breakage. Fire Safety Science-Proceedings of the Seventh International Symposium. Worcester, Massachusetts, USA: IAFSS, p. 3–22

[28] MJ Skelly, RJ Roby, CL Beyler (1991). An experimental investigation of glass breakage in compartment fires. J Fire Prot Eng, 3(1): 25–34

[29] K Harada, A Enomoto, K Uede, T Wakamatsu (2000). An experimental study on glass cracking and fallout by radiant heat exposure. Fire Safety Science-Proceedings of the Sixth International Symposium. IAFSS, pp. 1063–74

[30] Y Wang, Q Wang, G Shao, H Chen, J Sun, L He (2014). Experimental study on critical breaking stress of float glass under elevated temperature. Mater Des, 60: 41–9

[31] Y Wang, Y Zhang, Q Wang, Y Yang, J Sun (2018). The effect of glass panel dimension on the fire response of glass façades. Construction and Building Materials, 181: 588–597

[32] Y Wang, Q Wang, Y Su, J Sun, L He, KM Liew (2015). Fracture behavior of framing coated glass curtain walls under fire conditions. Fire Saf J, 75: 45–58

[33] Y Wang, Y Zhang, Q Wang, Y Yang, J Sun (2018). Sensitivity analysis of influencing factors on glass façade breakage in fire. Fire Safety Journal, 98: 38–47

[34] TJ Shields, GWH Silcock, M Flood (2002). Performance of a single glazing assembly exposed to a fire in the centre of an enclosure. Fire Mater., 26(2): 51–75

[35] W Chow, W Hung, Y Gao, G Zou, H Dong (2007). Experimental study on smoke movement leading to glass damages in double-skinned façade. Constr Build Mater, 21(3): 556–566

[36] Y Wang, Q Wang, G Shao, H Chen, Y Su, J Sun, L He, KM Liew (2014). Fracture behavior of a four-point fixed glass curtain wall under fire conditions. Fire Safety Journal, 67: 24–34

[37] MS Klassen, JA Sutula, MM Holton, RJ Roby, T Izbicki (2006). Transmission through and breakage of multi-pane glazing due to radiant exposure. Fire Technology, 42(2): 79–107

[38] A Vedrtnam, C Bedon, MA Youssef, M Wamiq, A Sabsabi, S Chaturvedi (2020). Experimental and Numerical Structural Assessment of Transparent and Tinted Glass during Fire Exposure. Construction and Building Materials, Volume 250, 118918, doi: 10.1016/j.conbuildmat.2020.118918

[39] M Debuyser, J Sjöström, D Lange, D Honfi, D Sonck, J Belis (2017). Behaviour of monolithic and laminated glass exposed to radiant heating. Constr Build Mater, 130: 212–29

[40] M Kozlowski, C Bedon, D Honfi (2018). Numerical analysis and 1D/2D sensitivity study for monolithic and laminated structural glass elements under thermal exposure. Materials, 11(8): 1447, doi: 10.3390/ma11081447

[41] prEN thstr:2004.Glass in Buildings—Thermal Stress Capitulation Method; CEN: Brussels, Belgium, 2004

[42] C Bedon (2017). Structural Glass Systems under Fire: Overview of Design Issues, Experimental Research, and Developments. Advances in Civil Engineering, 2017, 1–18. doi: 10.1155/2017/2120570

[43] M Kozłowski, C Bedon (2021). Sensitivity to Input Parameters of Failure Detection Methods for Out-of-Plane Loaded Glass Panels in Fire. Fire 2021, 4(5), https://doi.org/10.3390/fire4010005

[44] C Bedon, C Louter (2018). Thermo-mechanical numerical modelling of structural glass under fire-preliminary considerations and comparisons. Proceedings of Challenging Glass Conference, pp. 513–524

[45] J Sjöström, M Kozłowski, D Honfi, D Lange, J Albrektsson, P Lenk, J Eriksson (2020). Fire Resistance Testing of a Timber-Glass Composite Beam. International Journal of Structural Glass and Advanced Materials Research 2020, 4(1): 24-40, doi: 10.3844/sgamrsp.2020.24.40

[46] ASTM D790-03 - Standard Test Methods for Flexural Properties of Unreinforced and Reinforced Plastics and Electrical Insulating Materials, ASTM International, West Conshohocken, PA, 2003, www.astm.org

[47] L Galuppi, GF Royer-Carfagni (2012). Effective thickness of laminated glass beams: New expression via a variational approach. Engineering Structures, 38: 53–67

[48] Simulia, ABAQUS computer software, Providence, RI, USA

[49] IV Ivanov (2006). Analysis, modelling, and optimization of laminated glasses as plane beam. International Journal of Solids and Structures, 43(22–23): 6887-6907

[50] PA Hooper, BRK Blackman, KP Dear (2012). The mechanical behaviour of poly(vinyl butyral) at different strain magnitudes and strain rates. J Mater Sci 47, 3564–3576

[51] T Hána, M Vokáč, K Machalická, M Eliášová (2018). Material Properties of Polymeric Interlayers under Static and Dynamic Loading with Respect to the Temperature. Challenging Glass 6 -Conference on Architectural and Structural Applications of Glass. Louter, Bos, Belis, Veer, Nijsse (Eds.), Delft University of Technology, May 2018, https://doi.org/10.7480/cgc.6.2164

[52] W Stevels, P D'Haene, P Zhang, S Haldeman (2016). A Comparison of Different Methodologies for PVB Interlayer Modulus Characterization. Challenging Glass 5 – Conference on Architectural and Structural Applications of Glass Belis, Bos & Louter (Eds.), Ghent University, June 2016, ISBN 978-90-825-2680-6

[53] C Louter, C Bedon, M Kozłowski, A Nussbaumer (2021). Structural response of fire-exposed laminated glass beams under sustained loads; exploratory experiments and FE-Simulations. Fire Safety Journal, Volume 123, July 2021, 103353, https://doi.org/10.1016/j.firesaf.2021.103353

[54] M. Quinn Brewster, Thermal Radiative Transfer and Properties, Wiley (1992), March 1992, ISBN: 978-0-471-53982-7

[55] Galuppi L, Royer-Carfagni G, The post-breakage response of laminated heat-treated glass under in plane and out of plane loading, Composites Part B (2018), doi: 10.1016/ j.compositesb.2018.04.005.